CURRENT SCIENCE AND TECHNOLOGY
E-ISSN: 2785-8804
VOLUME 5, ISSUE 1, 2025, 48-60
DOI: https://doi.org/10.15282/cst.v5i1.10632

RESEARCH ARTICLE

Enhanced photocatalytic activity of zinc oxide nanostructures grown by the hot-tube thermal evaporation method

U.H. Hashim, N.N. Hamid, S. Suhaimi*, N.A. Taib

Nano Energy Lab (NEL), Department of Applied Physics, Faculty of Science and Technology, Universiti Sains Islam Malaysia, 71800, Negeri Sembilan, Malaysia

Abstract - As photocatalysis has become a promising solution for water treatment to remove toxic substances caused by the textile industry, many researchers are finding ways to improve the photocatalysis process. Over time, zinc oxide (ZnO) which has many attractive properties despite being low-cost, has attracted researchers. However, ZnO also has room for improvement and there are many other ways to enhance ZnO as a photocatalyst to be more efficient in water treatment. In this study, nanostructure ZnO is proposed to be used instead of bulk ZnO. Among the several ways available to synthesise ZnO nanowires, this research advocated employing the hot-tube thermal evaporation approach. Instead of the normal thermal evaporation method, other problems might occur to grow well-aligned ZnO nanowires which can be overcome by using a tube. In this study, the influence of oxygen gas flow rates at 5%, 10%, and 25% is also examined. The Energy-Dispersive X-ray analysis indicated that the sample contains a high proportion of zinc and oxygen, suggesting a high-purity ZnO composition. The highest strong diffraction peak for X-ray Diffraction of ZnO was found at (101), which showed a single crystalline hexagonal structure with an optimal growth direction in the c-axis. As from the photocatalytic activity, all three samples are observed from the photodegradation efficiency. In summary, the sample with a 25% oxygen gas flow rate was selected as the optimal condition for synthesising a homogeneous ZnO surface with high crystallinity via a hot-tube thermal evaporation process, yielding the best photodegradation efficiency in the photocatalysis process.

Article History
Received : 28 April 2024
Revised : 12 November 2024
Accepted : 23 December 2024
Published : 30 June 2025

Keywords
Zinc oxide
Thermal evaporation
Gas flow rate
Photocatalysis

1. Introduction

Water treatment has been crucial for decades, enabling the recycling of contaminated water, increasing the world's water supply, and reducing water pollution. Among the various recommended water treatment alternatives, photocatalysis stands out as the best option due to its low cost and great efficiency [1]. This water treatment addresses water contaminated with organic dyes. Organic dyes are in high demand because they are extensively employed in the rubber, textile, and plastic industries. It is also among the most prevalent contaminants in wastewater [2]. Due to the dye's potential toxicity and visibility in aquatic systems, they have caused serious environmental damage. Several physicochemical approaches for detoxifying synthetic colours from textile effluents have been proposed and reported in the literature. Nanotechnology has long been a promising multidisciplinary field, flourishing across many disciplines of science, biosciences, and technology. Heterogeneous photocatalytic degradation techniques using semiconductor nanoparticles as photocatalysts are essential for the complete mineralisation of a wide range of organic dyes and chemicals, thereby directly addressing environmental problems. Zinc oxide (ZnO) has been proposed as an alternative to conventional treatments for removing dye contaminants from water. ZnO has been extensively employed as an oxide semiconductor photocatalyst owing to its electrical and photonic properties and oxidation resistance.

Since its earliest realisation, photocatalysis using titanium dioxide (TiO_2) has attracted considerable interest. However, TiO_2 has two key drawbacks: low activity under visible light, which accounts for a large portion of the solar spectrum, and poor photoelectrical efficiency owing to light scattering by TiO_2. ZnO, in contrast, has the photocatalytic ability to break down organic dyes to CO_2 and H_2O, as well as the ability to absorb a higher proportion of the UV spectrum and more light quanta than TiO_2 [3]. ZnO has emerged as a remarkable and promising semiconductor in recent years, owing to its intriguing multi-properties, such as a wide band gap of 3.37 eV, high binding energy of 60 meV, and low cost. However, due to the large band gap, photocatalytic efficiency cannot be optimised. It may also result in significant energy waste. As a result, it is not the best candidate for photocatalysis. To solve these concerns, this study advocated for the use of ZnO nanowires rather than conventional ZnO. In general, specific surface area and surface defects, particularly oxygen vacancies, are two critical parameters that directly affect the photocatalytic activity of metal oxide semiconductors. ZnO nanowires have a naturally high surface-to-volume ratio, making them effective photocatalysts with direct activity enhancement. Lastly, there are many approaches to synthesise ZnO nanostructures, including the hydrothermal method, carbothermal reduction method, thermal evaporation method, and others. In thermal evaporation, several issues may arise when growing well-aligned ZnO nanowires, as a silicon (Si) substrate is commonly used in this method. However, the Si substrate exhibits greater residual strain. This study employs an improved method, hot-tube thermal evaporation (HTTE), to produce ZnO nanowires under intermediate growth conditions. This technique requires only simple instrumentation that can be readily assembled in the laboratory. This should provide an adequate background and general context for the

*CORRESPONDING AUTHOR | M Hanafi | ✉ nafy_fnd@yahoo.com
© 2025 The Author(s). Published by Universiti Malaysia Pahang Al-Sultan Abdullah Press. This is an open access article under the CC BY-NC 4.0 license

work, explaining its significance and indicating why it should be of interest to researchers—without delving into a detailed literature survey or summarising the results. State the objectives of the study at the end of this section.

2. Materials and Methods

2.1 Hot-Tube Thermal Evaporation Setup

In the absence of a catalyst, thermal evaporation was employed to create ZnO nanowires. In a quartz tube, ZnO nanostructures are fabricated. The pump was connected to one side of the quartz tube, while the other served as the gas intake, connected to the gas supply. Subsequently, the silicon (Si) substrate was inserted into the furnace for ZnO nanostructured growth. Figure 1 illustrates the schematic diagram of the hot-tube thermal evaporation setup, both in the quartz tube and in the entire system. Figure 1(a) illustrates the detailed arrangement within the quartz tube used in the hot-tube thermal evaporation process. It highlights the positioning of the substrate, the source material and the temperature gradients that are essential for the evaporation process. Concurrently, the entire system, as illustrated in Figure 1(b), is equipped with a variety of valves, including ball, check, and gate valves, to control gas flow throughout operation. The amount of gas moving through the system is then measured using a mass flow controller (MI-C). The rotary pump and Pirani gauge are placed on the substrate side of the quartz tube to establish and monitor the vacuum status throughout the system.

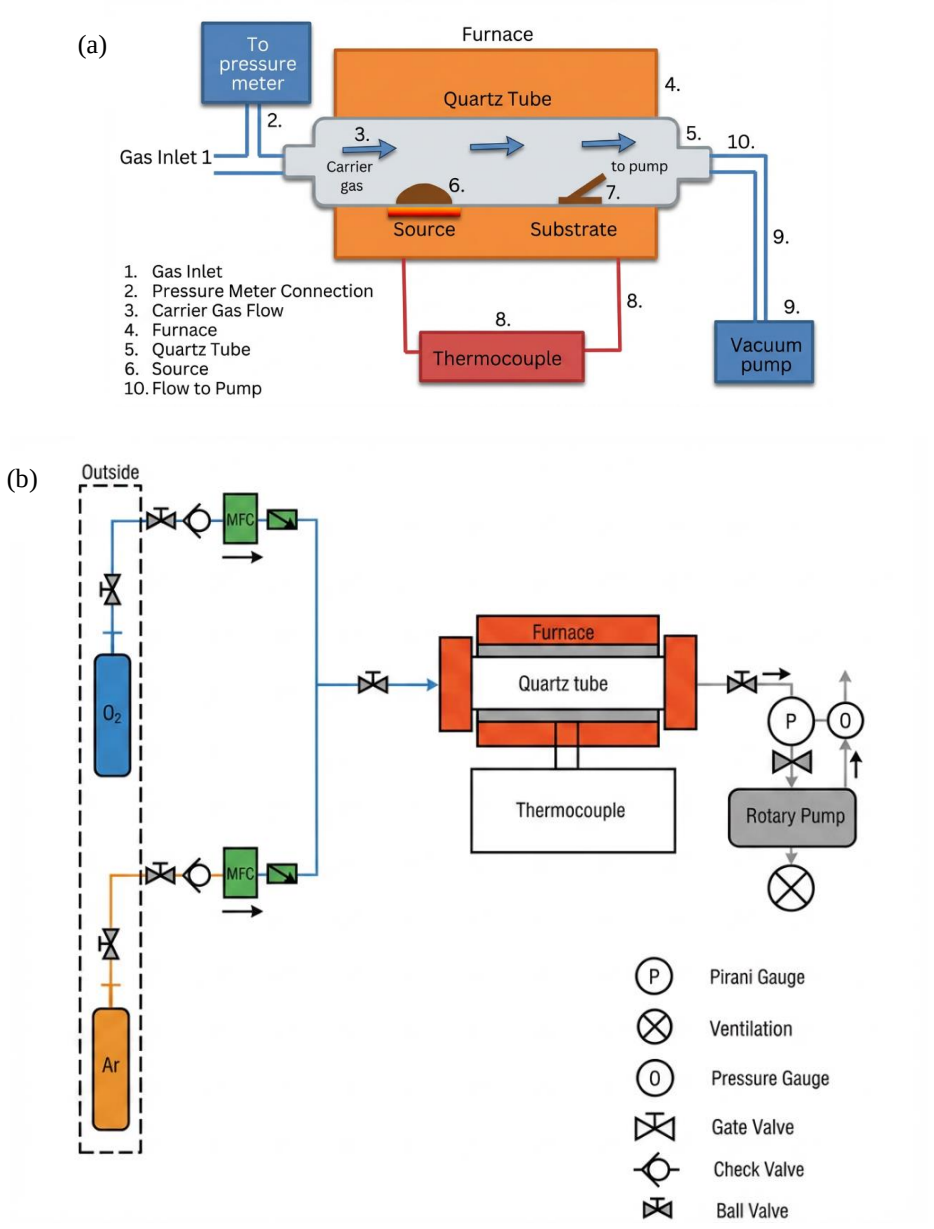


Figure 1. Hot-tube thermal evaporation set up (a) in the quartz tube (b) for the whole system [4]

2.2 Growing ZnO Nanowires

High-purity zinc powder (99.99%) from Sigma-Aldrich, USA, and O_2 (oxygen) are required for the growth of ZnO nanostructures. Zn powder was weighed and ground in a mortar to ensure homogeneous mixing. The mixed powder, the source material, is placed in an Alumina boat and inserted into the quartz tube. The distance between the powder mixture

and the prepared Si substrate is set at 18 cm, with the quartz tube in the centre. The rotary pump attached to the furnace on the substrate side is then evacuated by opening the argon gas line valve. This step is required to remove any undesired gases that may have been present in the previous stages of the process. After 5 minutes, turn on the vacuum system and open the oxygen gas valve. Table 1 presents a detailed breakdown of gas flow rates used in the experiment, including the percentage composition and the actual volume (in standard cubic centimetres per minute, cc/min) of each gas. High-purity argon, the carrier gas, and oxygen, the reactive gas, are delivered into the chamber and mixed. The argon and oxygen flow rates are varied across three samples: 10 cc/min of O_2, 20 cc/min of O_2, and 50 cc/min of O_2, corresponding to 5%, 10%, and 25% of the total gas flow, respectively. The total flow rate for both gases must be 200 cc/min. As Zn has a melting point of 600 ℃, a temperature of 800 ℃ was chosen to maintain the system just above the melting point of the metals, ensuring a steady supply of Zn vapour during the deposition process. The experiment's timer is set to 150 minutes. The oxygen supply shut off, and the tube furnace cooled under argon before the samples were extracted.

Table 1. Percentage and volume of gas flow rate

Sample	Oxygen gas		Argon gas	
	Percentage	Flow rate	Percentage	Flow rate
Sample 1	5 %	10 cc/min	95 %	190 cc/min
Sample 2	10 %	20 cc/min	90 %	180 cc/min
Sample 3	25 %	50 cc/min	75 %	150 cc/min

2.3 Photocatalysis Setup

In this study, methylene blue (MB) is employed to depict the pollutant. Photocatalysis is observed in the photodegradation of MB using a ZnO photocatalyst prepared via the HTTE technique. At the beginning of the photocatalysis method, 50 mL of 10 ppm MB from R&M Marketing, Essex, U.K., was placed in a conical flask. The formed ZnO photocatalyst was placed in the MB solution beaker. The heated plate stirrer is activated, and the solution is agitated in the dark for 15 minutes to attain MB absorption-desorption equilibrium. To produce a dark atmosphere, an isolated box with a UV lamp was employed. After 15 minutes, 4 mL of MB was collected and labelled as T_0. The UV light was projected over the solution containing the ZnO nanowire catalyst for the duration of the experiment (90, 120, 150, or 180 minutes), with continual stirring. Three hours of photocatalysis with a commercial ZnO catalyst that has not been changed were investigated. The UV light used has a wavelength of 365 nm. Figure 2 represents the experimental apparatus used for the photodegradation of methylene blue dye. It details the arrangement of the light source, the dye solution container, and the stirrer. All samples were examined and analysed using a UV-Vis spectrometer.

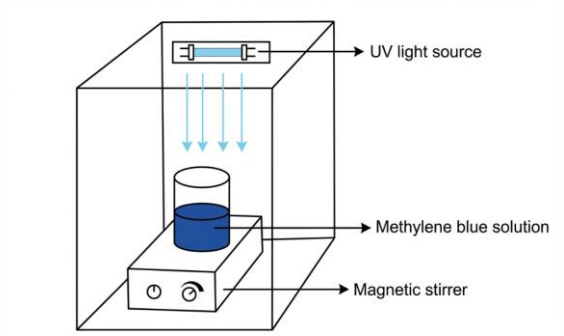


Figure 2. Experimental set-up of methylene blue dye photodegradation [7]

A Varian Cary® 50 UV-Vis Spectrophotometer (North America) is used to analyse the absorption spectra and changes in λ_{max} of the dyes. While the photocatalytic activity efficiency was calculated using Eq. (1):

$$D\% = \frac{A_0 - A}{A_0} \times 100 \quad (1)$$

where A_0 is the initial dye absorbance and A is the final dye absorbance.
The standard concentration of methylene blue calculated using Eq. (2):

$$M_1V_1 = M_2V_2 \quad (2)$$

To calculate the photodegradation of methylene blue, Eq. (3) was used:

$$C_{pdwc} = C_{tot} - C_{bal} - C_{ads} - C_{sd} - C_{pdxc} \quad (3)$$

where, C_{pdwc} is the concentration of photodegradation with catalyst, C_{tot} is the total concentration, C_{bal} is the concentration balance, C_{ads} is the concentration adsorption (without light)//MB without light, C_{sd} is the concentration self-desorption (with light)//MB with light and C_{pdxc} is the concentration photodegradation without catalyst.

3. Results and Discussion

3.1 Field Emission Scanning Electron Microscope Analysis

In this study, the morphology of the ZnO nanowire structure grown on ZnO was examined using FESEM. Figure 3 shows that FESEM provides a top-view image of the nanowires formed on the surface. ZnO low-dimensional nanostructures have short photo-generated carrier migration paths. This leads to rapid carrier migration, enhancing photocatalytic activity [8]. The results show that the ZnO nanostructures are evenly distributed across the silicon substrate surface. However, they vary with the flow rate of oxygen gas, as shown in Figures 3, 4, and 5, which are 10 cc/min, 20 cc/min, and 50 cc/min, respectively. The three samples have distinct morphologies, indicating that oxygen gas plays a significant role in their structural properties.

In Figure 3, the oxygen gas flow rate is the lowest, only 10 cc/min, and the argon gas flow rate is 190 cc/min. The sample consists of larger nanostructures and other nanoclusters. Aggregated or clustered nanostructures may reduce the effective surface area and hinder photocatalytic activity [9]. The presence of multiple growth stages in the ZnO nanostructure reflects its structural growth [10]. For this oxygen gas flow rate, this structure is most likely promoted by the peculiar nano-seed structure. This growth rate and process follow the vapour-liquid-solid mechanism, which explains the growth of ZnO nanowires. This is because no catalyst is used during growth, and no catalyst particles are detected at the ZnO nanowire tips. It appears the growth of the ZnO straight nanowires reported here occurs via a vapour–solid mechanism [11]. As the oxygen gas flow rate is increased to 20 cc/min (10%) and the argon gas flow rate decreased to 90%, the FESEM image in Figure 4 shows that the synthesised ZnO has a predominant granular morphology. The introduction of shape can explain changes in shape as its amount increases [12]-[14]. Figure 5 clearly shows that the entire substrate surface was covered with high-density, randomly oriented ZnO nanostructures when the sample was grown with 25% O_2 and 75% Ar. The dense ZnO has nanostructures with lengths of 200-220 nm. The uniform distribution of the nanostructures is likely to enhance their photocatalytic performance, as well-dispersed ZnO nanostructures ensure uniform exposure to light and efficient photon utilisation [9].

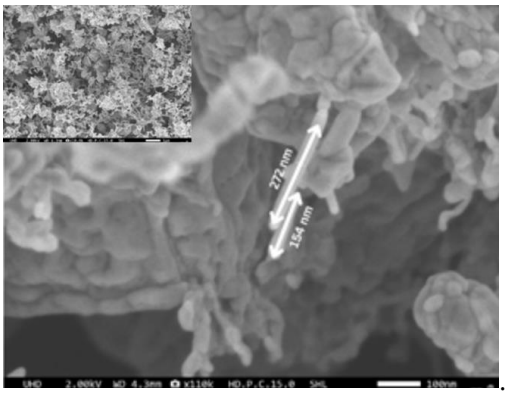


Figure 3. ZnO nanostructures with 10 cc/min of oxygen gas flow rate at 10 kx magnification and 110 kx magnification

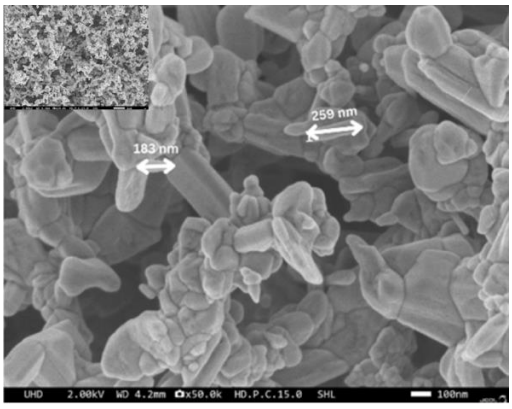


Figure 4. ZnO nanostructures with 20 cc/min of oxygen gas flow rate at 10 kx magnification and 50 kx magnification

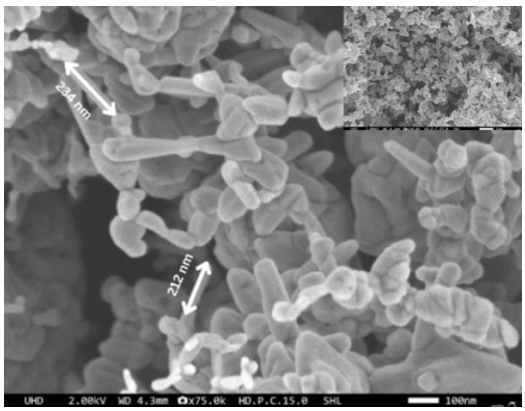
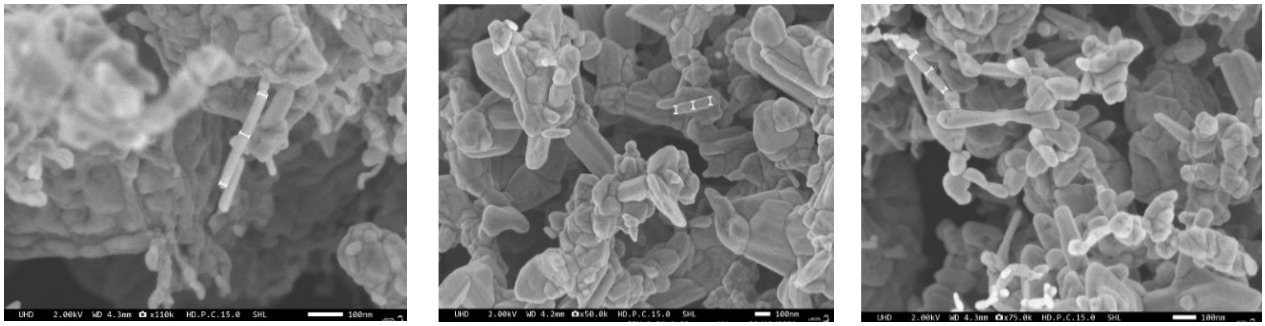


Figure 5. ZnO nanostructures with 50 cc/min of oxygen gas flow rate at 10 kx magnification and 75 kx magnification

The tapering factor (TF) is suggested for precisely quantifying tapering. The lowest value of TF is zero (0.00), indicating that the diameter along the nanowire is uniform, while a greater value of TF indicates a larger diameter deviation. The TF value was computed using the diameters of the nanostructure's tip, middle, and bottom, as illustrated in Figure 6.



(a) (b) (c)

Figure 6. The diameter measurement of the tip, middle, and bottom of different O_2 flow rates (a) 10cc/min (b) 20 cc/min (c) 50 cc/min

Equation (5) could be utilised to compute the TF value. Table 2 summarises the average length, average diameters at the tip, middle, and bottom, and the tapering factor of ZnO nanowires synthesised at various oxygen gas flow rates.

$$d_i = \frac{dT_i + dM_i + dB_i}{3} \tag{4}$$

$$TF = \frac{|dT_i - d_i| + |dM_i - d_i| + |dB_i - d_i|}{3} \tag{5}$$

where TF is the tapering factor (TF ≥ 0.00), d_i is the average diameter of the individual nanowire, dT_i is the diameter of the tip, dM_i is the diameter of the middle and dB_i is the diameter of the bottom.

Table 2. The average length and diameter of the tip, middle, and bottom of ZnO nanostructures grown at various oxygen flow rates, as well as the tapering factor

O_2 flow rate (cc/min)	d_i (nm)	dT (nm)	dM (nm)	dB (nm)	TF
10	213	20	26	21	2.43
20	221	23	27	25	1.33
50	223	19	20	20	0.89

Based on the graph in Figure 7, as the percentage of oxygen gas flow rate in the synthesised ZnO increases, the average length of the ZnO nanowires increases, indicating an optimal value. Higher oxygen percentages allow more oxygen to be present, which may help supersaturate ZnO in its gaseous form, resulting in longer structures. This discovery is consistent with the proposed relationship between gas-phase supersaturation and the final shape of the proposed nanostructures [15]. As mentioned before, a larger nanostructure size yields a higher surface-to-volume ratio, thereby increasing the number of active sites and, consequently, the reaction efficiency. On the other hand, Figure 8 shows that the higher oxygen gas flow rate yields the best tapering factor. The tapering factor for sample 3, which delivers 50 cc/min of oxygen gas, is 0.89, the closest to 0.00, indicating the nanowire is uniform. Thus, it was affirmed that varying gas flow rate plays a crucial part in controlling the nucleation and growth of ZnO nanostructures.

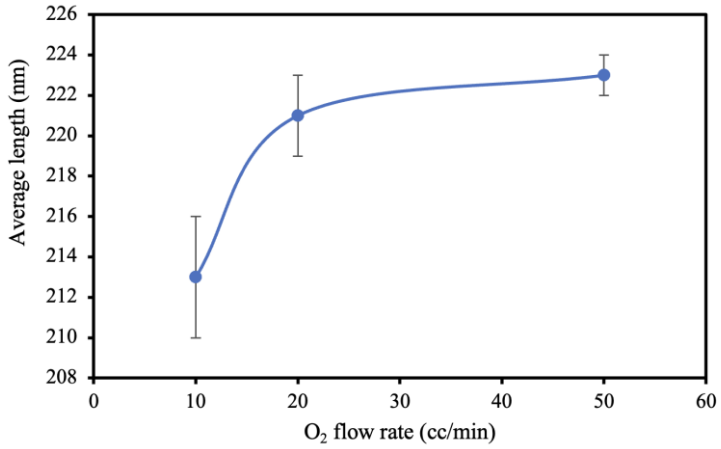


Figure 7. The average length against the oxygen flow rate of ZnO nanostructure (cc/min)

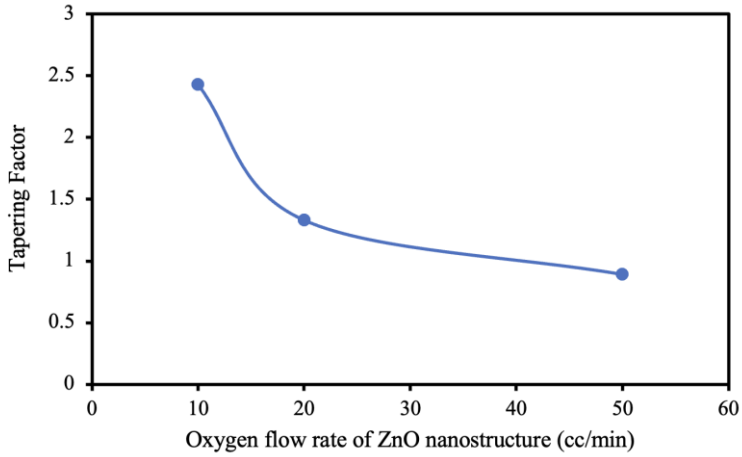


Figure 8. The graph of the tapering factor against the oxygen flow rate of ZnO nanostructure (cc/min)

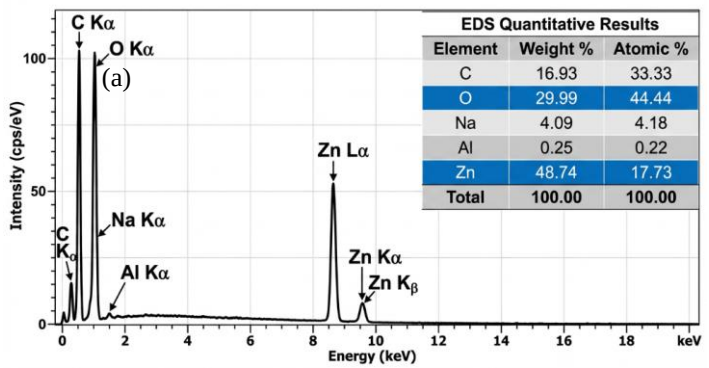
3.2 Morphology Analysis

EDX was used to identify the specified location in the FESEM sample. Following FESEM analysis, EDX analysis reveals the sample's composition, including the nanowires. This analysis was carried out to identify the constituents of the synthesised ZnO. As observed in the spectra in Figure 9, the element that the nanostructure possesses the most in all samples is zinc, followed by oxygen. There is a presence of carbon (C) in the spectra for each sample that may be resulting from a heating process. The presence of silicon (Si) is likely due to the silicon substrate on which the ZnO is grown. The elements sodium (Na) and aluminium (Al) could have come from the substrate and the source holder, respectively. Nevertheless, the obtained ZnO sample is considered high quality because Zn and O accounted for the highest percentages in all three samples, compared to other elements. Figures 10-12 illustrate elemental mapping for all three samples at varying oxygen gas flow rates. Figure 9 shows that the elements are uniformly distributed and not concentrated at a single spot, indicating that all samples possess well-grown ZnO nanostructures.

3.3 X-ray Diffraction Analysis

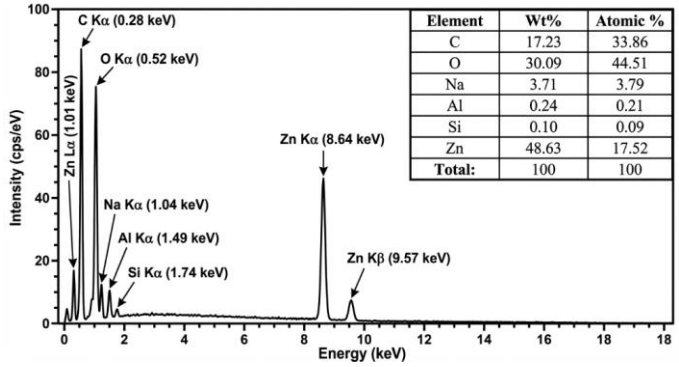
To further verify the enhancement of the sample's structural properties, XRD analysis was conducted to confirm the crystal structure of the ZnO nanostructure. Figure 13 displays three representative XRD patterns, which show a few sharp peaks attributed to the high-purity ZnO nanocrystalline phase. All of the samples vary in the amount of oxygen gas, as mentioned before. Samples 1, 2, and 3 have 5%, 10%, and 25% of the oxygen gas flow rate, respectively. The highest peak for each sample was recorded, with an orientation of (101) on the plane, and a mean angle of 2. The diffraction peaks are in good agreement with the hexagonal wurtzite structure of ZnO. The sharp peak in the (101) plane suggests that the synthesised ZnO was highly oriented, implying that the c-axis grew perpendicular to the substrate surface. The favoured c-axis orientation boosts the final properties [16].

On the other hand, Sample 2, which used 10% of the oxygen gas flow rate, has a low peak, indicating low crystallinity. Thus, we observe that gas flow rates influence ZnO crystallinity, which is linked to nucleation and growth mechanisms. Crystallinity refers to the degree of order in the arrangement of atoms within a crystal lattice. In the study, Sample 3, containing 25% oxygen gas, exhibited the highest crystallinity, as it was the strongest sample. Higher crystallinity generally leads to better photocatalytic efficiency [17]. The XRD results were further analysed to determine the average crystallite size of the ZnO produced.



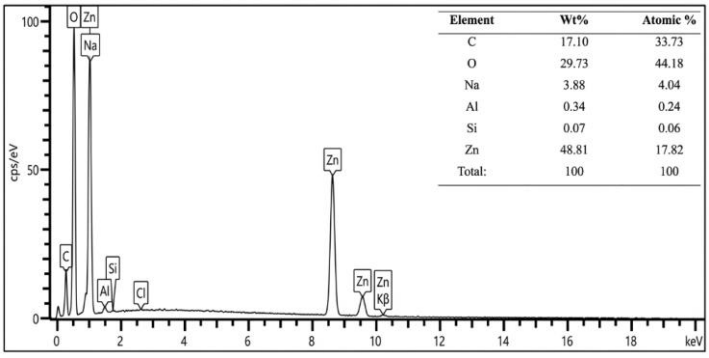
EDS Quantitative Results		
Element	Weight %	Atomic %
C	16.93	33.33
O	29.99	44.44
Na	4.09	4.18
Al	0.25	0.22
Zn	48.74	17.73
Total	100.00	100.00

(a)



Element	Wt%	Atomic %
C	17.23	33.86
O	30.09	44.51
Na	3.71	3.79
Al	0.24	0.21
Si	0.10	0.09
Zn	48.63	17.52
Total:	100	100

(b)



Element	Wt%	Atomic %
C	17.10	33.73
O	29.73	44.18
Na	3.88	4.04
Al	0.34	0.24
Si	0.07	0.06
Zn	48.81	17.82
Total:	100	100

(c)

Figure 9. EDX Spectra with different O_2 flow rate (a) 10 cc/min (b) 20 cc/min (c) 50 cc/min

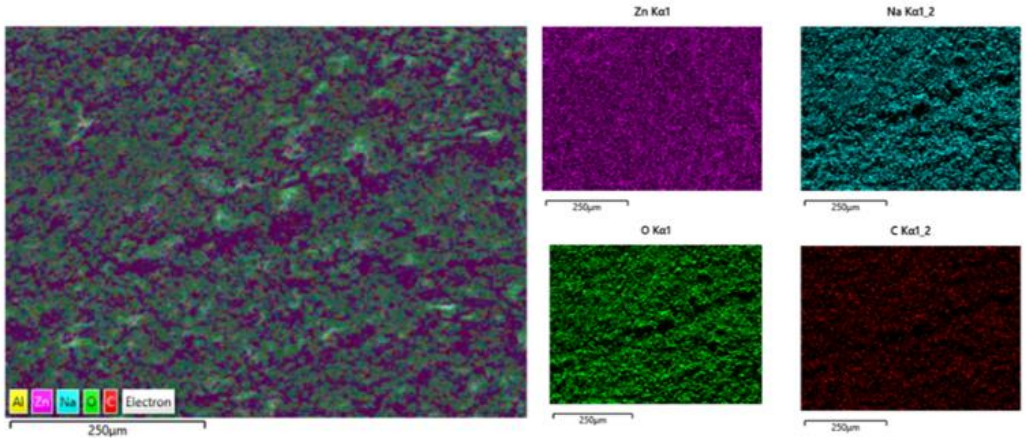


Figure 10. The 5% O_2 flow rate ZnO EDX mapping of the overall mapping and the elemental mapping

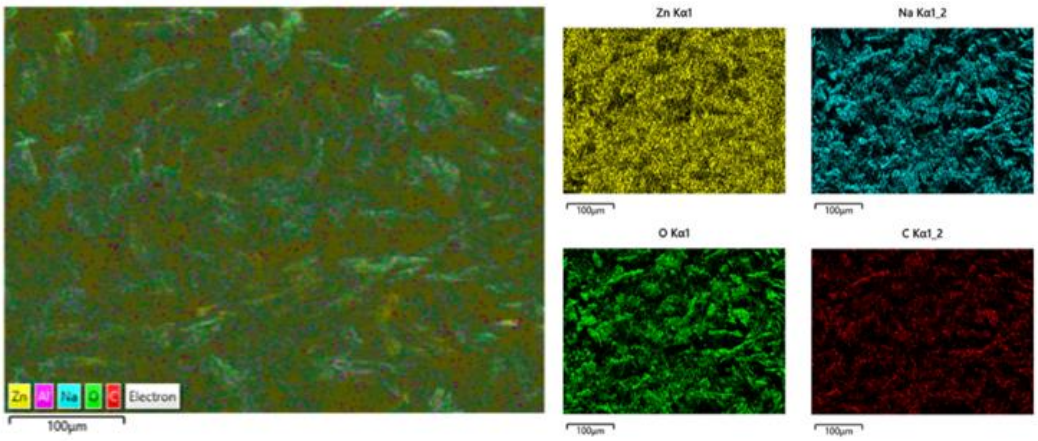


Figure 11. The 10% O_2 flow rate ZnO EDX mapping of the overall mapping and the elemental mapping

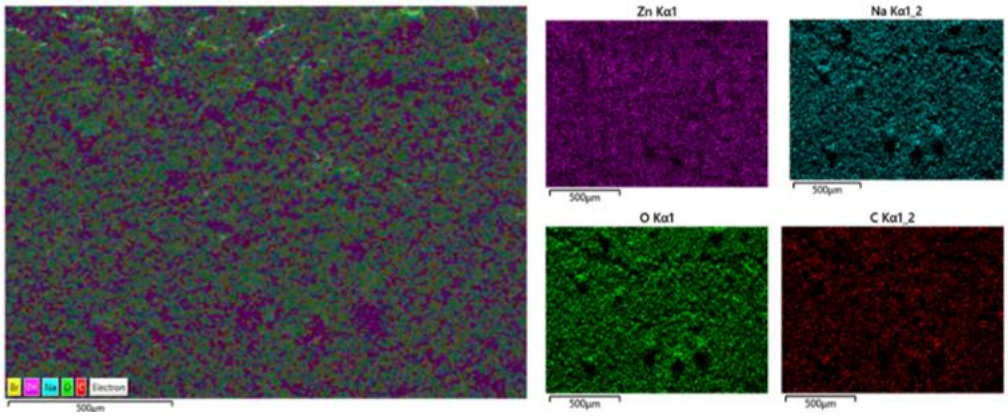


Figure 12. The 25% O_2 flow rate, ZnO EDX mapping of the overall mapping, and the elemental mapping

The crystalline size (D) of the films is estimated using Scherrer's equation and the plane of the Zincite phase using Eq.(5):

$$D = \frac{K\lambda}{\beta cos\theta} \tag{5}$$

where D is the crystalline size, K is 0.9, 0.154056 nm is the mean wavelength of Cu Kα radiation and is the full-width half maximum of the Bragg peak measured at the Bragg angle (rad). Table 3 shows that the average crystallite size was 37.02 nm, 68.31 nm, and 26.72 nm for samples 1, 2, and 3, respectively. The value of D increased as the O_2 gas flow rate increased from 5% to 10%, but then decreased as it further increased to 25%. A smaller crystallite size is preferable, as smaller crystallites have a higher surface area, providing more active sites for photocatalytic reactions and thereby increasing photocatalytic activity through efficient charge transfer. This is due to increased particle agglomeration on the surface of the synthesised ZnO in sample 2. The agglomeration of nanoparticles can be observed in the FESEM analysis in section 3.1. Table 4 is intended to compare the ZnO from the JCPDS library. From the table, it is clear that all three samples are comparable and show only a small difference, around 2%. Thus, it can be said that the synthesised ZnO possess a good characteristic for the crystallographic part.

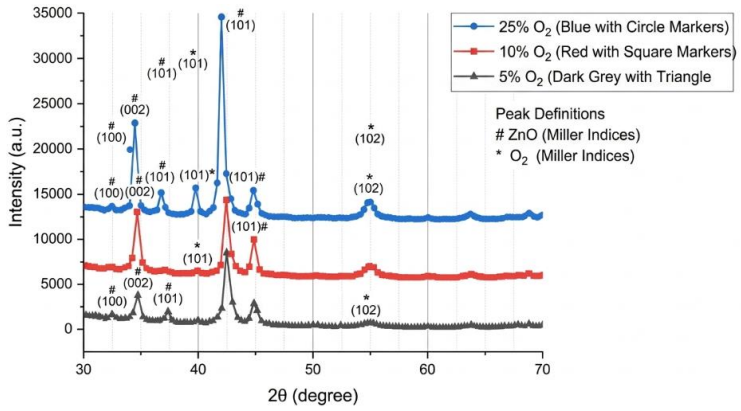


Figure 13. XRD Spectra of synthesised ZnO nanowires with varied O_2 flow rate

Table 3. Measurement and structural calculation of ZnO nanostructures for 5%, 10% and 25% of oxygen gas

Sample	Oxygen gas (%)	hkl plane	Lattice spacing, d	2$\boldsymbol{\theta}$(°)	a (Å)	c (Å)	Crystallite size, D (nm)
S1	5	(101)	2.2530	44.039	3.186	5.171	37.020
S2	10	(101)	2.5239	43.843	3.209	5.170	68.307
S3	25	(101)	2.5368	44.074	3.218	5.150	26.724

Table 4. The XRD crystallographic data and lattice parameter of JCPDS and the varied oxygen percentage samples

Samples	c (Å)	a (Å)	Volume (Å)	c/a
ZnO JCPDS	3.249	5.205	47.592	1.602
S1 (5% O_2)	3.186	5.171	45.458	1.623
S1 (10% O_2)	3.209	5.170	46.114	1.611
S1 (25% O_2)	3.218	5.150	46.194	1.600

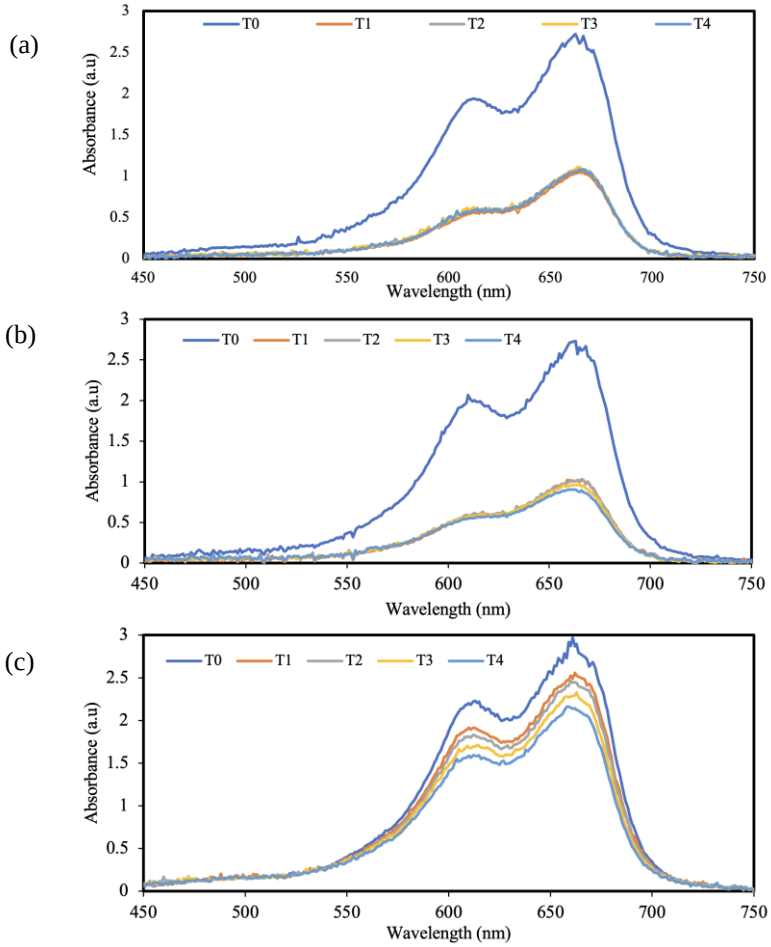


Figure 14. UV-Vis spectra with different O_2 flow rates (a) 10 cc/min, (b) 20 cc/min, (c) 50 cc/min

3.4 Photocatalysis Reaction Analysis

Once the structural properties were confirmed, the study proceeded to observe the photocatalytic activity, which was subsequently analysed using UV-Vis spectroscopy. UV-Vis refers to the absorption or reflectance of molecules in the ultraviolet-visible region by using light from visible and adjacent ranges. Besides, from the analysis, the photodegradation percentage and efficiency of ZnO nanowires as photocatalysts can be observed by using Eq. (2), as well as the concentration of the photodegradation with the photocatalyst after the photocatalysis process by using Eq. (3). 4 mL of methylene blue dye is taken at the start of the experiment, which is labelled as T_0. Starting at 90 minutes, another 4 mL of the methylene blue dye is added until 180 minutes. The solutions taken at 90 minutes, 120 minutes, 150 minutes, and 180 minutes are labelled as T_1, T_2, T_3, and T_4, respectively. Figure 14 depicts the time-dependent absorption spectra of MB aqueous solutions when exposed to visible light in the presence of ZnO nanowires. The highest peak among the three samples was at 662 nm and was later chosen to monitor the photocatalytic degradation process. The balance concentration, photodegradation concentration with catalyst, percentage of photodegradation, and the percentage removal of MB dye by ZnO nanowires grown are summarised in Tables 5-7 for each sample. Figures 15-16 were based on Table 5. From the

graph in Figure 15, the balance concentration of the methylene blue dye decreases over time, as shown in the pattern. The concentration of methylene blue started at 22.94782 ppm and, by the end of the reaction, the remaining concentration was only 14.77183 ppm.

Table 5. The summary of photodegradation of methylene blue data over time for 5% oxygen gas flow rate ZnO

Time	Cbal (ppm)	Photodegradation (%)
0	22.94782	0.00000
90	17.73657	18.30782
120	16.68702	22.88149
150	16.09479	25.46225
180	14.77183	31.22732

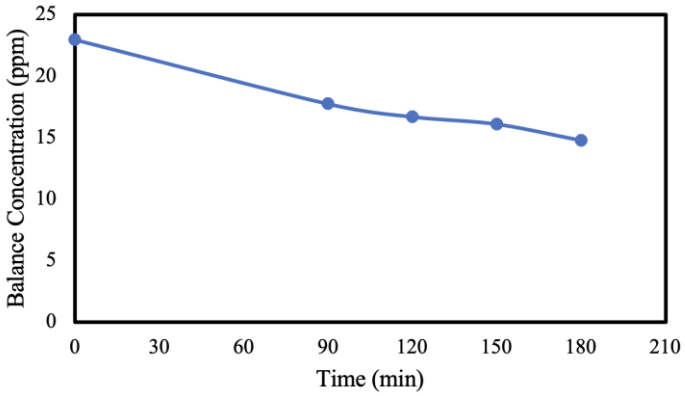


Figure 15. Balance concentration against time for 5% oxygen gas flow rate ZnO

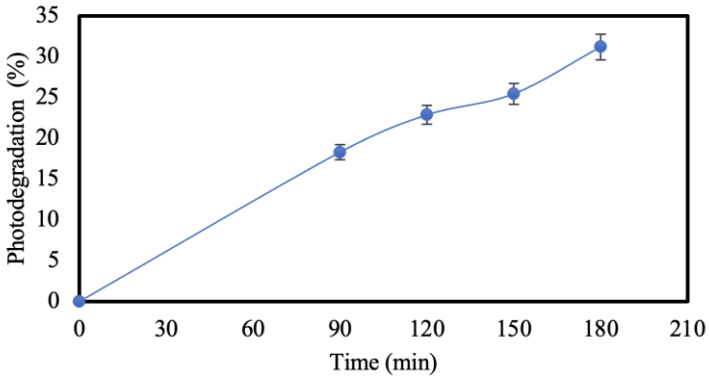


Figure 16. Photodegradation percentage against time for 5% oxygen gas flow rate ZnO

Figure 16 shows an increasing pattern of photodegradation percentage. As time increases, the photodegradation also increases. By the end of the reaction, the photodegradation percentage increased to 31.22%. The synthesised ZnO nanostructure with a 5% oxygen gas flow rate is a good photocatalyst and may be a viable option for wastewater treatment. Next, Figure 17 shows a decreasing pattern in the balance concentration of the methylene blue dye over time. The initial concentration of 20.86345 ppm decreased to 8.139946 ppm, indicating a significant trend. This result was better supported by the graph in Figure 18, which shows the increase in the photodegradation percentage during the photocatalysis reaction of the methylene blue dye, which represents the pollutant in the wastewater. Compared to the ZnO nanostructure with a 5% oxygen gas flow rate, this sample with a 10% oxygen gas flow rate performs better.

Table 6. The summary of photodegradation of methylene blue data over time for 10% oxygen gas flow rate ZnO

Time	Cbal (ppm)	Photodegradation (%)
0	20.863450	0.00000
90	8.544535	54.20443
120	8.473383	54.54546
150	8.222565	55.74766
10	8.139946	56.14365

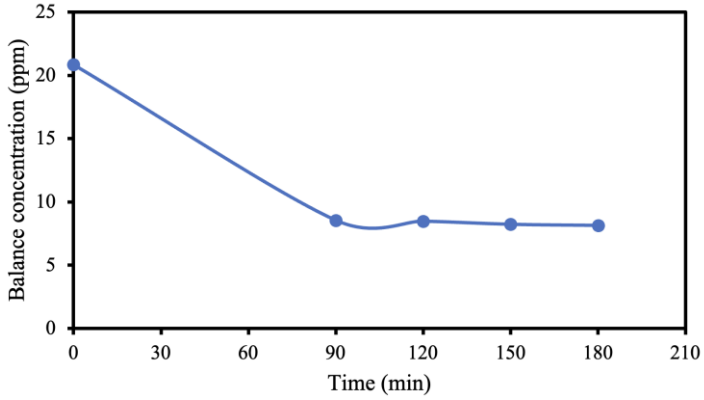


Figure 17. Balance concentration against time for 10% oxygen gas flow rate ZnO

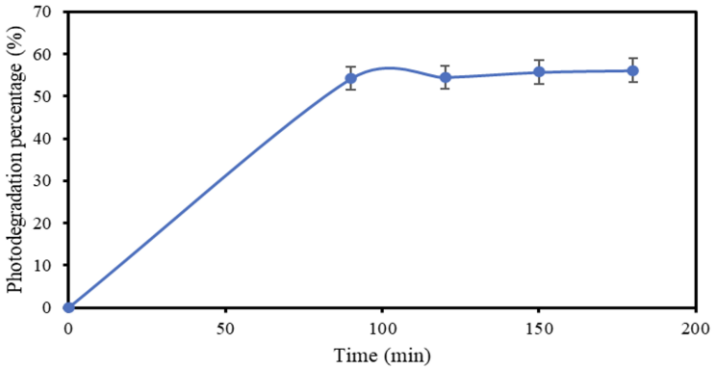


Figure 18. Photodegradation percentage against time for 10% oxygen gas flow rate ZnO

Lastly, Figures 19-20 show the balance concentration over time and the graph of photodegradation percentage over time, respectively. At the beginning of the experiment, the methylene blue dye concentration is 20.25544 ppm. Then it decreases gradually to a concentration of 5.614666 ppm after 180 minutes. Then, the graph of photodegradation percentage shown in Figure 20 increases linearly until 67.29% by the end of the reaction. The efficiency of photocatalysis increases as the oxygen gas flow rate increases, while the balance concentration decreases. Based on the photocatalysis analysis, sample 3, which has a 25% oxygen gas flow rate, shows the best performance, achieving approximately 67% photodegradation, the highest among the samples tested. It clearly shows that the sample has ideal structural properties, such as a small tapering factor (0.89 in FESEM analysis) and a well-distributed structure, with approximately 48% Zn in EDX analysis. The smallest crystallite size, *D*, affects the photodegradation process, in which the role of the nanostructures as a photocatalyst is well-played.

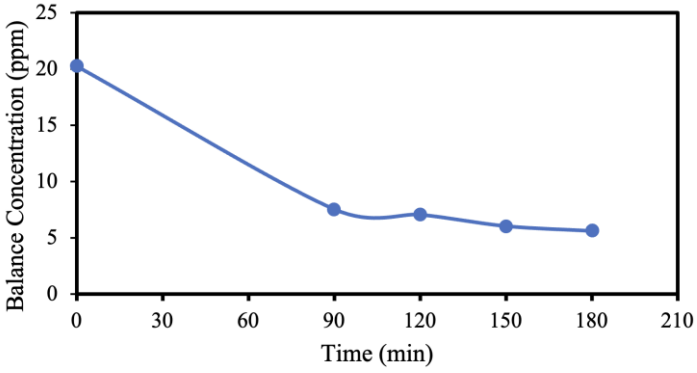


Figure 19. Graph of balance concentration (ppm) against the time (min) for 25% oxygen gas flow rate ZnO

Table 7. The summary of photodegradation of methylene blue data over time for 25% oxygen gas flow rate ZnO

Time	Cbal (ppm)	Percentage Photodegradation (%)
0	20.255440	0.00000
90	7.540887	57.78472
120	7.062245	60.14775
150	6.042643	65.18147
180	5.614666	67.29438

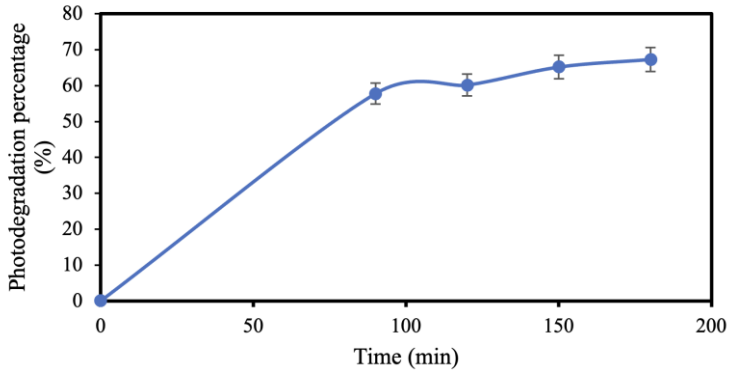


Figure 20. Photodegradation percentage against time for 25% oxygen gas flow rate ZnO

4. Conclusions

The ZnO nanowires were grown by thermal evaporation at 800 °C using oxygen concentrations of 5%, 10%, and 25%. Based on FESEM results, the ZnO nanostructures ranged from 150 nm to 250 nm, and their size decreased as the oxygen percentage increased. The average length of sample three with 25% O_2 is the shortest among those with 5% O_2. According to the XRD data, the ZnO structures are extremely crystalline. Several ZnO nanowires were discovered, and the nanostructures were found to be distributed across the surface of the silicon substrate. In this study, the photocatalytic degradation of methylene blue is observed in all three samples. The sample with the highest photodegradation efficiency is sample three, which yields 67.3%, compared with 31.2% and 56.1% for samples one and two, respectively. In summary, the optimal oxygen percentage for synthesising ZnO nanostructures is 25%, in accordance with the study's scope. It can also be concluded that increasing the oxygen content above 25% further alters the sample's morphology.

Acknowledgements

The authors express their gratitude to Universiti Sains Islam Malaysia and the Faculty of Science & Technology, USIM, which provided the laboratory facilities required for the experimental work.

Funding

This work was supported by Universiti Sains Islam Malaysia (PPPI/FST/0121/USIM/15521).

Declaration of Competing Interest

The author declares no conflicts of interest.

CRediT Authorship Contribution Statement

U.H. Hashim (Methodology; Data curation; Writing – original draft; Resources)
N. Hamid ((Methodology; Data curation; Writing – original draft; Resources)
S. Suhaimi (Conceptualization; Writing – review & editing; Funding acquisition; Supervision)
A. Mat Taib (Conceptualization; Writing – review & editing; Supervision)

Availability of Data and Materials

The data supporting this study's findings are available on request from the corresponding author.

Ethics Declarations

This study did not involve human participants or animals. Ethical approval was therefore not required.

Generative Artificial Intelligence Declarations

The authors claim that artificially intelligent-assisted technologies, such as generative AI, were not used to generate content, ideas, or theories. We have just utilised AI to enhance readability and refine the language. This was used with extreme human control and oversight. The authors take full responsibility for reviewing and approving the content.

References

[1] D. Li and W. Shi, "Recent developments in visible-light photocatalytic degradation of antibiotics," *Cuihua Xuebao/Chinese Journal of Catalysis*, vol. 37, no. 6, pp. 792–799, 2016.
[2] C. Ma, Z. Zhou, H. Wei, Z. Yang, Z. Wang, and Y. Zhang, "Rapid large-scale preparation of ZnO nanowires for photocatalytic application," *Nanoscale Research Letters*, vol. 6, no. 1, p. 536, 2011.
[3] A.D. Folawewo and M.D. Bala, "Nanocomposite zinc oxide-based photocatalysts: recent developments in their use for the treatment of dye-polluted wastewater," *Water*, vol. 14, no. 23, pp. 3899–3899, 2022.

[4] S. Sakrani, P.O. Amin, and S. Suhaimi, "Zinc oxide nanowires synthesized using a hot tube thermal evaporation under intermediate heating period," *Malaysian Journal of Fundamental and Applied Sciences*, vol. 9, no. 4, pp. 201-205, 2014.
[5] M. Scimeca, S. Bischetti, Harpreet Kaur Lamsira, R. Bonfiglio, and E. Bonanno, "Energy dispersive X-ray (EDX) microanalysis: A powerful tool in biomedical research and diagnosis," *European Journal of Histochemistry*, vol. 62, no. 1, p. 2841, 2018.
[6] A. Polini and F. Yang, "Physicochemical characterization of nanofiber composites," in *Nanofiber Composites for Biomedical Applications*, Amsterdam, The Netherlands: Elsevier, 2017, pp. 97–115.
[7] A. Das, Nikhil S.K, and R.G. Nair, "Influence of surface morphology on photocatalytic performance of zinc oxide: A review," *Nano-Structures & Nano-Objects*, vol. 19, pp. 100353–100353, 2019.
[8] P. Porrawatkul, R. Pimsen, A. Kuyyogsuy, P. Rattanaburi, and P. Nuengmatcha, "Morphology-dependent photocatalytic performance of ZnO nanostructures in organic dye and antibiotic degradation," *International Journal of Environmental Science and Technology*, vol. 21, no. 11, pp.7397-7414, 2024.
[9] E. Albiter, A.S. Merlano, E. Rojas, J.M. Barrera-Andrade, Á. Salazar, and M.A. Valenzuela, "Synthesis, characterization, and photocatalytic performance of ZnO–graphene nanocomposites: A review," *Journal of Composites Science*, vol. 5, no. 1, p. 4, 2020.
[10] M. Hassan, L. Jiaji, P. Lee, and R.S. Rawat, "Catalyst free growth of ZnO thin film nanostructures on Si substrate by thermal evaporation," *Applied Physics. A, Materials Science & Processing*, vol. 127, no. 7, p. 553, 2021.
[11] J. Li and H. Li, "Physical and electrical performance of vapor–solid grown ZnO straight nanowires," *Nanoscale Research Letters*, vol. 4, no. 2, p. 165, 2008.
[12] N. Rusli, Masahiro Tanikawa, M. Mahmood, K. Yasui, and A. Hashim, "Growth of high-density zinc oxide nanorods on porous silicon by thermal evaporation," *Materials*, vol. 5, no. 12, pp. 2817–2832, 2012.
[13] A. Alkahlout, N. Al Dahoudi, I. Grobelsek, M. Jilavi, and W. de Oliveira, "Synthesis and characterization of aluminum doped zinc oxide nanostructures via hydrothermal route," *Journal of Materials*, vol. 2014, pp. 1–8, 2014.
[14] N. Hamid, S. Suhaimi, M.Z Othman, and W. Zakiah, "A review on thermal evaporation method to synthesis zinc oxide as photocatalytic material," *Nano hybrids and composites*, vol. 31, pp. 55–63, 2021.
[15] P.M. Winkler and P.E. Wagner, "Characterization techniques for heterogeneous nucleation from the gas phase," *Journal of aerosol science*, vol. 159, pp. 105875–105875, 2022.
[16] M.F. Malek, M.H. Mamat, Z. Khusaimi, M.Z. Sahdan, M.Z. Musa, A.R. Zainun et al., "Sonicated sol–gel preparation of nanoparticulate ZnO thin films with various deposition speeds: The highly preferred c-axis (002) orientation enhances the final properties," *Journal of alloys and compounds*, vol. 582, pp. 12–21, 2014.
[17] J. Liu, W. Fu, Y. Liao, J. Fan, and Q. Xiang, "Recent advances in crystalline carbon nitride for photocatalysis," *Journal of Materials Science and Technology*, vol. 91, pp. 224–240, 2021.